case where internal (inclusion) pressure is lower than external (confining) pressure (*21*). Our melt interpretation no doubt needs further testing, but we believe it is the most plausible explanation as compared to other hypotheses (*22*).

It is remarkable that the cristobalite was able to resist reconstructive transformation to β-quartz during denudation and cooling of the rock, considering that the Adirondack Highlands cooled at a rate of −1.5°C per million years after the peak of granulite facies metamorphism, staying at temperatures in excess of 600°C for 100 million years (*23*). The cristobalite may have survived because of the absence of water, which serves to catalyze reconstructive transformation. Water may not have had access to these rocks until mid- to upper-levels of the crust were reached during uplift, but it is unlikely that significant diffusion of water back into the garnets occurred at these temperatures. The absence of water was also suggested to explain the preservation of coesite inclusions in garnet (and other phases) from ultrahigh-pressure rocks (*24*, *25*). The preservation of cristobalite in rocks cooled slowly from high temperature implies that, in the absence of water, the activation energy for the β-cristobalite to β-quartz transformation is high.

REFERENCES AND NOTES

1. C. Frondel, *The System of Mineralogy*, vol. 3, *Silica Minerals* (Wiley, New York, ed. 7, 1962).
2. J. A. Klasik, *Science* **189**, 631 (1975).
3. D. S. Beljankin and V. P. Petrov, *Am. Mineral.* **23**, 153 (1938).
4. A. Van Valkenburg and B. F. Buie, *ibid.* **30**, 526 (1945).
5. W. W. Schmahl, I. P. Swainson, M. T. Dove, A. Graeme-Barber, *Z. Kristallogr.* **201**, 125 (1992).
6. W. W. Schmahl, *Eur. J. Mineral.* **5**, 377 (1993).
7. V. G. Hill and R. Roy, *J. Am. Ceram. Soc.* **41**, 532 (1958).
8. L. H. Cohen and W. Klement Jr., *Philos. Mag. A* **39**, 399 (1979).
9. J. B. Bates, *J. Chem. Phys.* **57**, 4042 (1972).
10. D. de Waard, *J. Petrol.* **8**, 210 (1967); F. Luther, thesis, Lehigh University, Bethlehem, PA (1976).
11. R. G. Berman, *J. Petrol.* **29**, 445 (1988).
12. A. E. Ringwood and D. H. Green, *Tectonophysics* **3**, 383 (1966).
13. J. R. Holloway, *Geochim. Cosmochim. Acta* **37**, 651 (1973).
14. S. R. Bohlen *et al.*, *J. Petrol.* **26**, 971 (1985).
15. F. S. Spear and J. C. Markussen, *ibid.*, in press.
16. K. R. Hosieni *et al.*, *Am. Mineral.* **70**, 782 (1985).
17. S. Wen and H. Nekvasil, *ibid.* **79**, 316 (1994).
18. If this process occurred at $T \geq 910$°C, the melt would enter the tridymite stability field.
19. J. F. Schairer and N. L. Bowen, *Am. J. Sci.* **254**, 129 (1956).
20. L. Wang *et al.*, *Am. Mineral.* **81**, 706 (1996).
21. S. M. Sterner and R. J. Bodnar, *J. Metamorphic Geol.* **7**, 243 (1989); M. O. Vityk, R. J. Bodnar, V. Dudok, *Eur. J. Mineral.* **7**, 1071 (1995).
22. Other possible interpretations include (i) a garnet + β-cristobalite epitaxial relation, (ii) a devitrification product of glass inclusions, or (iii) an exsolution product of supersilicic garnet.
23. K. Mezger, C. M. Rawnsley, S. R. Bohlen, G. N. Hanson, *J. Geol.* **99**, 415 (1991).
24. C. Chopin, *Contrib. Mineral. Petrol.* **86**, 107 (1984); A. I. Okay, X. Shutong, A. M. C. Sengör, *Eur. J. Mineral.* **1**, 595 (1989); X. Wang, J. G. Liou, H. K. Mao, *Geology* **17**, 1085 (1989).
25. Unlike these occurrences of coesite, we did not observe marginal- or fracture-related replacement of cristobalite by α-quartz. The reason for this is unknown, but the two polymorphs did experience very different retrograde *PT* paths, which will affect the availability and diffusivity of water, as well as the compressibility and expansivity of the host and inclusion phases.

26. We thank D. Lindsley, F. Florence, and H. Nekvasil for help with this investigation, J. Ireland for technical assistance, B. Gravatt and J. Hunt for assistance in scanning electron microscopy and electron microprobe analysis, and P. Dunn and J. Post of the Smithsonian Institution for providing natural cristobalite for Raman analysis. Suggestions by P. Barton, G. Nord, and two anonymous reviewers greatly improved earlier versions of this manuscript.

30 October 1996; accepted 30 January 1997

Spatial Variability of Turbulent Mixing in the Abyssal Ocean

K. L. Polzin,* J. M. Toole, J. R. Ledwell, R. W. Schmitt

Ocean microstructure data show that turbulent mixing in the deep Brazil Basin of the South Atlantic Ocean is weak at all depths above smooth abyssal plains and the South American Continental Rise. The diapycnal diffusivity there was estimated to be less than or approximately equal to 0.1×10^{-4} meters squared per second. In contrast, mixing rates are large throughout the water column above the rough Mid-Atlantic Ridge, and the diffusivity deduced for the bottom-most 150 meters exceeds 5×10^{-4} meters squared per second. Such patterns in vertical mixing imply that abyssal circulations have complex spatial structures that are linked to the underlying bathymetry.

An outstanding question in oceanography is the intensity and spatial distribution of turbulent vertical mixing in the deep sea. Beyond affecting the dispersal of naturally occurring and anthropogenic substances, mixing relates through the buoyancy (heat) equation (*1*) and vorticity dynamics (*2*) to the intensity of upwelling and the horizontal circulation in the abyss. The rate of turbulent mixing at depth has previously been inferred from advective heat budgets constructed for deep, semi-enclosed basins (*3*, *4*). These studies report vertical diffusivity values (K) between 1×10^{-4} and 10×10^{-4} m^2 s^{-1}: one to two orders of magnitude greater than values deduced for the upper ocean interior from ocean microstructure data (*5*) and a tracer experiment (*6*), and from limited deep observations away from boundaries (*5*, *7*, *8*). Those few deep-ocean microstructure observations near rough bathymetry suggest that mixing there is much enhanced (*8*, *9*). To further examine the intensity, spatial distribution, and mechanisms of mixing in the deep ocean, we initiated a joint physical oceanographic and tracer study in the Brazil Basin of the South Atlantic Ocean. This area was chosen because a diffusivity estimate based on an abyssal heat budget was available for this region (*3*) and extensive data have recently been collected there as part of the World Ocean Circulation Experiment.

We made physical observations with a freely falling instrument, the High Resolution Profiler (HRP) (*10*). This device returns temperature, salinity, and horizontal velocity information as a function of depth, along with dissipation estimates of turbulent kinetic energy and temperature variance. We infer turbulent diffusivity from the dissipation estimates, using models that assume a balance between turbulent production and dissipation (*11*). An independent technique we used to study mixing involves tracking an inert chemical tracer that is injected on a deep density surface. We used SF_6, a weakly soluble compound detectable in sea water at concentrations of 10^{-16} M (*12*). Time-averaged estimates of diapycnal diffusivity inferred from observations of the tracer's vertical dispersion can be compared to the more instantaneous diffusivity estimates for temperature and buoyancy deduced from microstructure data.

During a cruise of the R/V *Seward Johnson* from January to February of 1996, we occupied 75 stations with the HRP at sites ranging between the 3900-m isobath off the coast of Brazil and the western flank of the Mid-Atlantic Ridge (MAR; Fig. 1). Most of the profiles reached to within 30 m of the bottom. The resulting microstructure observations reveal a deep-ocean mixing pattern that appears to be correlated to the underlying bathymetry (Fig. 2). Above the smooth abyssal plains of the central Brazil Basin and the gradual slopes of the South American continental rise, we observed

Woods Hole Oceanographic Institution, Woods Hole, MA 02543, USA.

*To whom correspondence should be addressed. E-mail: kpolzin@whoi.edu

low-intensity microstructure. Turbulent diffusivity values for the central Brazil Basin were about 0.1×10^{-4} m^2 s^{-1}. We observed just a slight enhancement in the mixing over the rise within 100 m of the bottom, most likely a result of boundary layer turbulence. These small dissipation estimates were surprising in that a bottom-intensified deep western boundary current flows above the rise (albeit at speeds of only about 2 cm s^{-1}) that has been implicated in mixing Brazil Basin waters (*13*). In contrast, turbulent dissipation rates were elevated one to two orders of magnitude above the rough flanks of the MAR, particularly within 300 m of the bottom.

We repeatedly sampled one spur of the MAR with the HRP between 3 and 20 February, 1996, a period encompassing both spring and neap tides. Turbulent diffusivity values in this region were consistently greater than 10^{-4} m^2 s^{-1} within 300 m of the bottom; within 150 m, some values exceeded 10^{-3} m^2 s^{-1} (Fig. 3). This region of rough topography was chosen as the tracer release site. Approximately 110 kg of SF_6 was released during an 8-day period on a density surface at about 4010 m depth near 21°40′S, 18°25′W (Fig. 1) (*14*). The initial root-mean-square vertical spread of the tracer relative to the target density surface, resulting from shifts in sensor calibration between tows, was about 9 m. Tracer concentration broadened in the 11 days after injection (Fig. 4). Application of a diffusion model (*15*) returned a diapycnal diffusivity value of $0.5 \times 10^{-4} \pm 0.5 \times 10^{-4}$ m^2 s^{-1}. On the basis of the 39 HRP stations made in this region, we estimate that K between 3960 and 4060 m was 0.3×10^{-4} to 0.6×10^{-4} m^2 s^{-1} (95% confidence bounds). Although a K value close to zero cannot be ruled out by the tracer data, the best estimate is consistent with those from the HRP.

The microstructure data show that mixing was enhanced throughout much of the water column in regions with rough topography. Turbulence supported directly by bottom stress is limited to boundary layers that are typically only tens of meters high. That mixing occurs remote from the bottom implicates wave processes that can transport energy up from the bottom. Steady and time-dependent bottom currents flowing over undulating bathymetry can generate internal waves that propagate up into the water column (*16*). Subsequent instability and breaking of such waves would provide an energy source for the turbulent mixing. Consistent with this idea, enhanced fine-scale shear and strain (*17*) were observed above rough bathymetry. We propose that the energy source for the internal waves supporting the mixing near the MAR is the barotropic tides impinging on the rough bathymetry of the ridge. (Mean

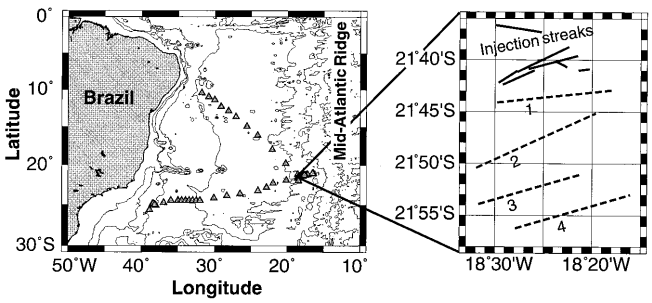

Fig. 1. Distribution of HRP stations (triangles) in the Brazil Basin of the South Atlantic Ocean. Isobaths greater than 2000-m depth are depicted with a contour interval of 1000 m. The expanded scale plot to right shows the ship tracks during injection of the SF_6 tracer (solid lines). The dashed lines mark the sampling tracks of the initial tracer survey.

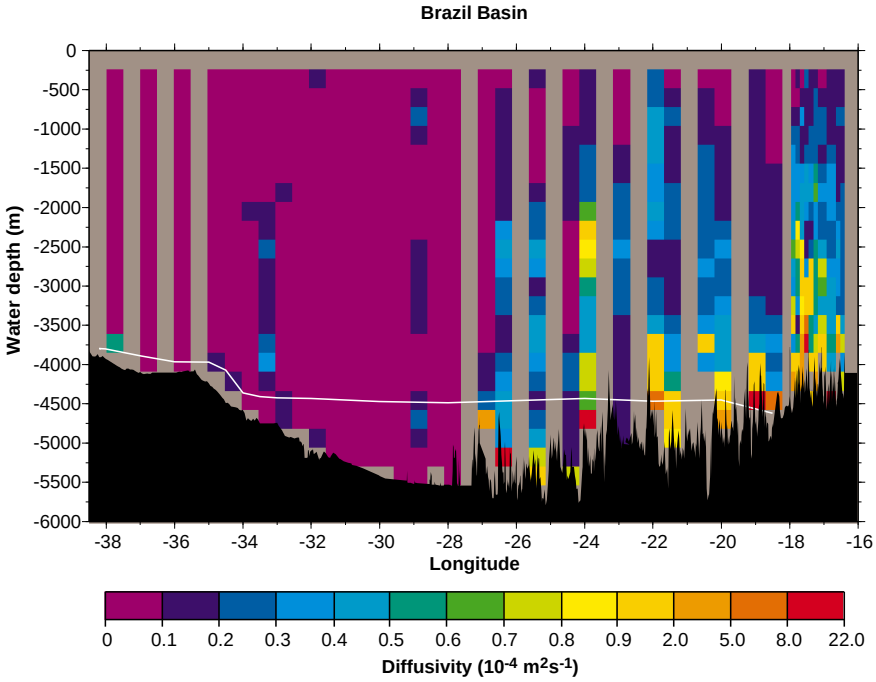

Fig. 2. Depth-longitude section of cross-isopycnal diffusivity in the Brazil Basin inferred from velocity microstructure observations. Note the nonuniform contour scale. Microstructure data from the two quasi-zonal transects have been combined without regard to latitude. The underway bathymetric data to 32°W is from the eastward track, the balance comes from the westward track. The white line marks the observed depth of the 0.8°C surface.

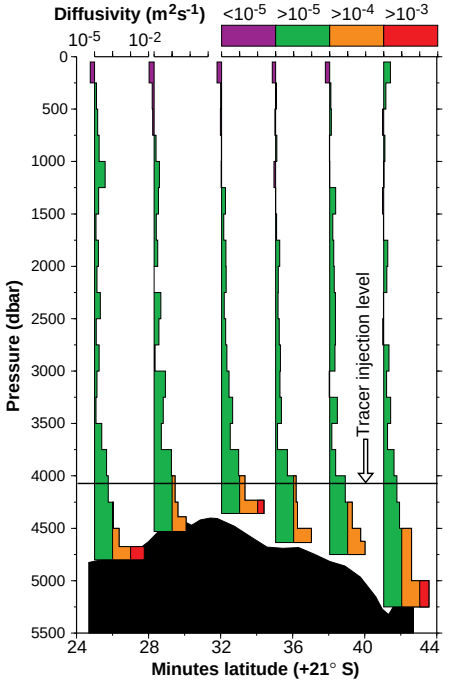

Fig. 3. Profiles of average cross-isopycnal diffusivity versus depth as a function of position relative to a spur of the MAR (whose bathymetry is shown versus latitude). Diffusivity profiles have been offset horizontally to roughly correspond to their physical position relative to the spur and are plotted on a logarithmic axis. The tick marks and color scheme denote decadal intervals, and the vertical reference lines denote $K = 10^{-5}$ m^2 s^{-1}. The 95% confidence intervals are roughly ±50% of the depicted estimates. The horizontal line marks the average depth at which the SF_6 tracer was injected.

and low-frequency currents appear to be weak in the eastern Brazil Basin.) If correct, given the ubiquitous nature of ocean tides, we expect the pattern of enhanced mixing associated with rough bathymetry to hold globally. Instability of bottom-reflected internal waves might also contribute to near-bottom mixing (*18*), particularly within the valleys between ridge spurs where wave energy can be focused (*19*). Mid-basin shear and strain intensities were, in contrast, at climatological levels for the background internal wave field (*20*), and signatures of internal wave reflection and associated mixing were not apparent in data from the gradually and smoothly sloping South American continental rise. Proximity to the bottom is seemingly not a sufficient condition for enhanced mixing in the deep ocean: the small-scale structure of the bottom appears key.

From a heat budget based on bottom-water transport estimates through the Vema Channel, Hogg *et al.* (*3*) deduced that the basin-averaged turbulent heat flux per unit area across the 0.8°C potential temperature surface was 2.0 W m^{-2}. Our observations come close to explaining this flux as the product of internal wave breaking in the eastern part of the basin (Table 1). The uncertainty reported for our flux value of 0.4 to 1.1 W m^{-2} does not include bias error. The estimate may be biased low (*21*). Additional mixing, not factored into our estimate, might also occur near the Vema Channel where the deep flow is greatly intensified by bathymetric constrictions, as has been observed within bottom waters flowing through the Romanche fracture zone (*22*). Considering all uncertainties, we judge it probable that mixing above rough bathymetry and at the Vema Channel is sufficiently intense to close the heat budget for the bottom waters in the Brazil Basin.

The corresponding mass budget for the waters below the 0.8°C surface (or nearly equivalently, σ_4 = 45.98 kg m^{-3}) (*23*) presents a puzzle. Hogg *et al.* (*3*) estimated a transport of 3.6 × 10^6 m^3 s^{-1} below σ_4 = 45.98 kg m^{-3} through the Vema Channel (*24*). Of this, approximately 0.2 × 10^6 m^3 s^{-1} escapes the Brazil Basin through the Romanche and Chain fracture zones (*25*), and approximately 1 × 10^6 m^3 s^{-1} exits through a channel situated on the equator at 35°W (*26*). Thus, at least 2 × 10^6 m^3 s^{-1} must upwell across the σ_4 = 45.98 kg m^{-3} surface within the Brazil Basin. The average diapycnal velocity based on a surface area of 5 × 10^{12} m^2 (*5*) is at least 4 × 10^{-7} m s^{-1}. However, we infer downwelling at a rate of –6 × 10^{-7} m s^{-1} where this surface lies above the rough ridge bathymetry, on the basis of the diapycnal advection-diffusion balance (*27*)

$$w^* = (\partial_z \rho)^{-1}\, \partial_z\, (K \partial_z \rho) = N^{-2}\, \partial_z(\Gamma\, \varepsilon)$$

where $N^2 = -g\rho^{-1}\, \partial_z \rho$ and the buoyancy flux has been related to the kinetic energy dissipation rate, ε, through an efficiency factor Γ (*11*), thought to be around 0.2 for turbulent mixing of stratified water. In our observations, the sign of $\partial_z\, \varepsilon$ determines the sign of w^*. This inferred downwelling acts to increase the volume of dense water. It is unlikely that the estimated sign of w^* will change with greater sampling: an enhancement of turbulent mixing at depth, above that characteristic of the upper ocean interior, is required to close the bottom-water heat budget, and the sense of this vertical gradient implies downwelling. How then is the mass budget within the deep Brazil Basin closed? We hypothesize that water is fluxed strongly upward across density surfaces in the many deep canyons that extend from the mid-ocean ridge crest. HRP profiles obtained within these canyons indicate a decreasing trend with depth for ε below the peaks of the local bathymetry (*28*), consistent with a positive diapycnal velocity. On a broad scale then, the fractured MAR might be viewed as a permeable, sloping boundary with sinks for the densest waters in the Brazil Basin at the depths of the canyon mouths and sources of water at depths about the canyon heads.

Our findings suggest that abyssal circulation patterns are far more complex than were described by Stommel and Arons (*2*) to demonstrate possible dynamical effects of deep upwelling. In the interior regions of the Brazil Basin characterized by smooth bathymetry, we find very weak mixing. As a dynamical consequence, the horizontal flow there must be nearly along lines of constant potential vorticity (*29*). Consistent with the effects of mixing over a sloping boundary (*30*), hydrographic sections spanning the Brazil Basin reveal deep isopycnals sloping down into the MAR (*13*). With a mid-depth level of no motion for the meridional velocity, the thermal wind relation implies a bottom-intensified flow directed toward the equator. This circulation is opposite to that deduced by Stommel and Arons (*2*) for uniform deep upwelling in an ocean with a flat bottom. In a link between flows at disparate spatial scales, our observations suggest that the structure and intensity of these basin-scale abyssal circulations are controlled by centimeter-scale turbulent mixing, itself dictated by kilometer-scale bathymetric relief and surface tides via the internal wave field.

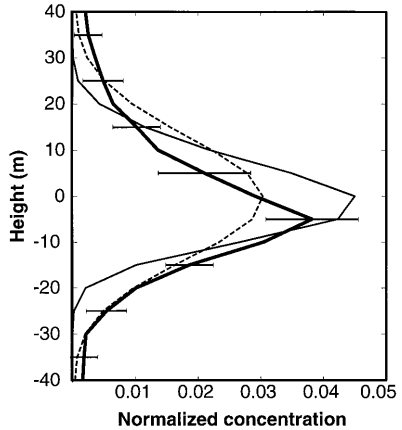

Fig. 4. Profiles of SF_6 concentration versus height above the target density surface. An array of integrating water samplers was towed along four tracks through the patch approximately 11 days after the injection (Fig. 1), guided by pop-up floats that had been deployed with the tracer. A rough integral of these concentration data suggests that 80 ± 20% of the deployed tracer was sampled. The bold solid line is the best estimate of the observed profile, the error bars giving ±1 standard error. The thin line is an estimate of the initial tracer distribution. The dashed line is the model result for K = 0.5 × 10^{-4} m^2 s^{-1} acting on the initial profile for 11 days. The concentration profiles have been normalized to give unity for the integral over height. The observed concentration profile will additionally serve as the initial condition for subsequent studies of the tracer dispersion.

Table 1. Estimation of the vertical turbulent heat flux across the potential temperature surface Θ = 0.8°C in the Brazil Basin. On the basis of the pattern of turbulent diffusivity (K) inferred from velocity microstructure data (Fig. 2), the basin was divided into three regions. For each, the vertical temperature gradient (Θ_z) and vertical diffusivity in a 100-m-thick interval bracketing the Θ = 0.8°C surface were estimated from the available HRP profiles in the respective regions. The turbulent heat flux per unit area was calculated as $Q = \rho c_p K \Theta_z$ with ρc_p = 4.1 × 10^6 J m^{-3} °C^{-1}. The intervals reported for K and Q are 95% confident bounds [as in (*8*)]. Area-mean estimates represent averages weighted by the reported area fractions; the basin-averaged K estimate is derived from the average Q and Θ_z values. The corresponding estimate provided by Hogg *et al.* (*3*) of the average vertical diffusivity at this surface is 3.3 × 10^{-4} m^2 s^{-1}.

Regions (number of profiles)	Area fraction	Θ_z (m°C m^{-1})	K (10^{-4} m^2 s^{-1})	Q (W m^{-2})
Western boundary (8)	0.05	3.6	0.2–0.7	0.3–1.0
Smooth bottom (16)	0.5	2.0	0.07–0.12	0.06–0.10
Rough bottom (20)	0.45	1.5	1.3–3.7	0.8–2.3
Area means or totals	1.0	1.9	0.5–1.5	0.4–1.1

REFERENCES AND NOTES

1. K. Wyrtki, *Deep-Sea Res.* **8**, 39 (1961); W. H. Munk, *ibid.* **13**, 207 (1966); A. E. Gargett, *J. Mar. Res.* **42**, 359 (1984).
2. H. Stommel and A. B. Arons, *Deep-Sea Res*. **6**, 140 (1960).
3. N. G. Hogg, P. Biscaye, W. Gardner, W. J. Schmitz, *J. Mar. Res*. (*Suppl.*) **40**, 231 (1982).
4. J. A. Whitehead and L. V. Worthington, *J. Geophys. Res.* **87**, 7903 (1982); P. M. Saunders, *J. Phys. Oceanogr*. **17**, 631 (1987); E. D. Barton and A. E. Hill, *Deep-Sea Res.* **36**, 1121 (1989); D. Roemmich, S. Hautala, D. Rudnick, *J. Geophys. Res.* **101**, 14039 (1996). Characteristic of these studies, a heat flux divergence is found, associated with bottom water flowing horizontally into a basin at a colder average temperature than it leaves by upwelling across isotherms. This divergence is presumed to be balanced by downward turbulent diffusion, with the requisite heat flux commonly expressed as a vertical diffusivity (*K*) multiplied by the mean vertical temperature gradient averaged horizontally over the basin.
5. M. C. Gregg, *J. Geophys. Res*. **94**, 9686 (1989); K. L. Polzin *et al*. *J. Phys. Oceanogr*. **25**, 306 (1995).
6. J. R. Ledwell, A. J. Watson, C. S. Law, *Nature* **364**, 701 (1993).
7. M. C. Gregg, *J. Phys. Oceanogr*. **7**, 436 (1977); J. N. Moum and T. R. Osborn, *ibid.* **16**, 1250 (1986); E. Kunze and T. B. Sanford, *ibid.* **26**, 2286 (1996).
8. J. M. Toole *et al*. *Science* **264**, 1120 (1994).
9. J. M. Toole, R. W. Schmitt, K. L. Polzin, E. Kunze, *J. Geophys. Res.* **102**, 947 (1997).
10. R. W. Schmitt *et al*. *J. Atmos. Ocean. Technol.* **5**, 484 (1988).
11. T. R. Osborn and C. S. Cox, *Geophys. Fluid Dyn*. **3**, 321 (1972); T. R. Osborn, *J. Phys. Oceanogr*. **10**, 83 (1980).
12. C. S. Law *et al*. *Mar. Chem.* **48**, 57 (1994).
13. X. Durrieu De Madron and G. Weatherly, *J. Mar. Res.* **52**, 583 (1994).
14. The tracer was injected into the ocean in a series of streaks by use of a tethered system that was towed behind the research vessel while being positioned vertically to remain within a few meters of a target density surface. Subsequent spread of the tracer was documented with water sample analysis conducted at sea with a gas chromatograph equipped with an electron capture detector (*12*).
15. J. R. Ledwell and A. Bratkovich, *J. Geophys. Res*. **100**, 20681 (1995).
16. T. H. Bell, *J. Fluid Mech.* **67**, 705 (1975); *J. Geophys. Res*. **80**, 320 (1975); P. G. Baines, *Deep-Sea Res*. **29**, 307 (1982); B. Sjöberg and A. Stigebrandt, *ibid.* **39** 269 (1992); S. A. Thorpe, *Proc. R. Soc. London Ser. A* **439**, 115 (1995).
17. Shear is the vertical variation of the horizontal velocity, and strain is the vertical gradient of vertical displacements, the latter inferred from variations in the separation between isopycnals.
18. O. M. Phillips, *The Dynamics of the Upper Ocean* (Cambridge Univ. Press, New York, ed. 2, 1977); C. C. Eriksen, *J. Geophys. Res.* **87**, 525 (1982); C. Garrett and D. Gilbert, in *Small-Scale Turbulence and Mixing in the Ocean, Proceedings of the 19th International Liege Colloquium on Ocean Hydrodynamics,* Liege, Belgium, 4 to 8 May 1987, J. C. J. Nihoul and B. M. Jamart, Eds. (Elsevier, New York, 1988), pp. 405–424.
19. F. S. Hotchkiss and C. Wunsch, *Deep-Sea Res*. **29**, 415 (1982).
20. C. Garrett and W. H. Munk, *J. Geophys. Res*. **80**, 291 (1975); J. L. Cairns and G. O. Williams, *ibid.* **81**, 1943 (1976).
21. Our estimate of the turbulent heat flux may be biased low for several reasons. First, more than 45% of the Brazil Basin might be categorized as "rough." The areal fractions assigned in Table 1 are based on our quasi-zonal sections. This breakdown does not, for example, include contributions to the rough-bottom category from the northern and southern boundaries of the Brazil Basin. Second, we most likely undersampled the mixing on the 0.8°C isotherm where it lies close to the bottom over rough bathymetry. Many of our HRP stations in the eastern Brazil Basin were atop ridge spurs and consequently did not sample temperatures this low. A reanalysis of the heat budget of Hogg *et al.* at somewhat warmer bounding temperature for which we have more microstructure observations could address this. Third, there may be regional variation in the intensity of the mixing above rough bathymetry due to changes in the small-scale bottom roughness, near-bottom currents, and stratification, all of which affect the generation of internal waves.
22. K. L. Polzin *et al*. *Nature* **380**, 54 (1996).
23. σ_4 is the potential density referenced to 4000 dbar.
24. Including the flow across the Santos Plateau and Hunter Channel, K. G. Speer and W. Zenk [*J. Phys. Oceanogr.* **23**, 2667 (1993)] obtained a somewhat larger transport of about 5×10^6 m^3 s^{-1}.
25. H. Mercier and K. Speer, in preparation.
26. M. Hall, personal communication.
27. The diapycnal velocity w^* was estimated as ~ 0.25 N^{-2} $\Delta\varepsilon/\Delta z$ over a 100-m interval about the 0.8°C potential isotherm. The neglected terms in this equation (set in a coordinate system aligned with the density field) associated with nonlinearities in the seawater equation of state that cause densification of water on mixing [T. McDougall, in *Proceedings of Hawaiian Winter Workshop*, SOEST Special Publication, 13 to 19 January 1991 (Univ. of Hawaii at Manoa, 1991), pp. 355–386] only exacerbate the problem with the mass budget closure.
28. Equivalently, in the vertical, our estimates of (K $\partial_z\rho$) peak about the crests of the MAR spurs and decrease with still greater depth within the canyons.
29. With a flat bottom and uniform stratification, the flow would be zonal. However, basin-scale bottom-depth variations [Speer and Zenk (*24*)] and eddy-driven horizontal recirculations extending from the western boundary [M. A. Spall, *J. Mar. Res.* **52**, 1051 (1994)] may strongly distort this interior circulation from simple zonal flow.
30. C. Wunsch, *Deep-Sea Res.* **17**, 293 (1970); L. Thompson and G. C. Johnson, *ibid.* **43**, 193 (1996).

31. We thank E. Montgomery, D. Wellwood, T. Donoghue, B. Guest, T. Bolmer, S. Sutherland, and L. St. Laurent for support of our field program and data analysis, and the officers and crew of the R/V *Seward Johnson*. Supported by the NSF Division of Ocean Sciences. The HRP was developed with support from the Department of Defense and the Office of Naval Research.

16 December 1996; accepted 10 February 1997

The Atmospheric Aerosol-Forming Potential of Whole Gasoline Vapor

J. R. Odum, T. P. W. Jungkamp, R. J. Griffin, R. C. Flagan, J. H. Seinfeld*

A series of sunlight-irradiated, smog-chamber experiments confirmed that the atmospheric organic aerosol formation potential of whole gasoline vapor can be accounted for solely in terms of the aromatic fraction of the fuel. The total amount of secondary organic aerosol produced from the atmospheric oxidation of whole gasoline vapor can be represented as the sum of the contributions of the individual aromatic molecular constituents of the fuel. The urban atmospheric, anthropogenic hydrocarbon profile is approximated well by evaporated whole gasoline, and thus these results suggest that it is possible to model atmospheric secondary organic aerosol formation.

Several recent epidemiologic studies have consistently reported increased daily mortality associated with exposure to fine particulate air pollution (*1, 2*). An important contribution to the atmospheric fine particulate burden, especially during severe urban smog episodes, is secondary organic aerosol (SOA) (*3*). Like ozone (O_3), SOA is formed from the atmospheric oxidation of organic compounds. Whereas the oxidation of most hydrocarbons contributes to O_3 formation, SOA is generally formed only from the oxidation of hydrocarbon molecules containing seven or more carbon atoms (*4*). To form SOA, oxidation products must have vapor pressures that are sufficiently low to enable them to partition into the particulate phase.

In an effort to achieve urban and regional O_3 abatement through the reduction of mass emissions of nonmethane hydrocarbons, the 1990 amendments to the U.S. Clean Air Act mandate the use of reformulated gasoline in motor vehicles. Several recent studies have suggested that a more effective approach to controlling urban O_3 associated with emissions from gasoline usage is to target the emissions of specific fuel components, rather than total nonmethane hydrocarbons, because of the extreme differences in the O_3-forming potential of the hundreds of individual compounds that constitute gasoline (*5*). Considering the common link between urban O_3 formation and SOA formation, this approach may also be an effective way to control SOA formation associated with emissions from gasoline usage.

Organic aerosol formation potentials depend on two factors: reactivity of the parent compound and volatility of the product species. The reactivity of the parent species can be directly measured by reaction rate constants. However, because atmospheric chemical reaction pathways for large hydrocarbon molecules are complex and the re-

J. R. Odum and T. P. W. Jungkamp, Department of Environmental Engineering Science, California Institute of Technology, Pasadena, CA 91125, USA.
R. J. Griffin, R. C. Flagan, J. H. Seinfeld, Department of Chemical Engineering, California Institute of Technology, Pasadena, CA 91125, USA.

*To whom correspondence should be addressed.